Supporting Information

In-situ morphological transformation and investigation of electrocatalytic properties of cobalt oxide nanostructures toward oxygen evolution

Sung-Fu Hung,[a] *Ching-Wei Tung,*[a] *Ting-Shan Chan,*[b,]**Hao Ming Chen*[a,]***

[a]Department of Chemistry, National Taiwan University, Taipei 106, Taiwan.

[b]National Synchrotron Radiation Research Center, Hsinchu 300, Taiwan.

Experimental Section

S1. Fabrication of cobalt oxide nano-needles on nickel foam and the morphological transformation of cobalt oxide

Co_3O_4 nano-needles were grown on nickel foam by means of chemical bath deposition and post-calcination.[1] In the deposition, the nickel foam, which was cleaned ultrasonically in acetone and subsequently ethanol, was suspended perpendicularly with an immersed area of 1 cm^2 in a sample vial at 90 °C for 3 hours. The typical precursor solution in the synthesis contained the mixture of 0.625 g of urea in 9.5 mL of deionized water and 0.5 mL of 3 M $Co(NO_3)_{2(aq)}$. After reaction, the obtained precursor film was rinsed thoroughly with deionized water and further calcinated at 300 °C for 2 hours with the heating rate of 2 °C/min. In order to investigate the morphological variation, the solutions of 3 M transition metal nitrate ($Ni(NO_3)_2$, $Cu(NO_3)_2$, $Zn(NO_3)_2$) were introduced into the reaction solution.

S2. Characterization

The morphologies and elemental analysis were investigated with field-emission scanning electron microscopy (FE-SEM, JEOL JSM-6700F) equipped energy dispersive X-ray spectroscopy (EDX, Oxford Instrument XMax 150 mm^2). The crystal structure was detected with X-ray diffractometer (XRD, Bruker D2 phaser). Selected area electron diffraction, energy dispersive X-ray spectroscopy, and high-resolution transmission electron microscopy images were characterized by TEM, JEOL JEM-2100F.

S3. Electrochemical measurements

Electrochemical properties were investigated on Bio-logic VSP potentiostat in a standard three-electrode setup using electrocatalyst modified nickel foam as the working electrode, a platinum plate as the counter electrode and a saturated calomel electrode (SCE) as the reference electrode. Aqueous solution of 1.0 M KOH (pH = 13.6) was used as the electrolyte. The potentials were converted to values relative to RHE based on the following equation: $E_{RHE} = E_{SCE} + 0.0591 \times pH + E^0_{SCE}$, where E^0_{SCE} is the standard potential of SCE relative to SHE at 25 °C (0.240 V). The working area of electrodes was fixed at 1 cm^2 for each experiment. Linear sweep voltammetry for oxygen evolution was collected at the scan rate of 1 mV/s with iR-correction. The electrochemical active surface area (ECSA) was measured from double-layer capacitance using cyclic voltammetry in a small potential range (0.25 V to 0.30 V vs. SCE), from which the double layer capacitance was determined from the slope of capacitive current at the midpoint of the scan range (0.275 V vs. SCE) versus

the scan rate according to $C_{dl}= I_{cap} /(dE/dt)$, where $C_{dl}$is the double layer capacitance and dE/dt is the scan rate. ECSAwas calculated through dividing the average specific capacitance of 40 μF/cm^{2}for transition metal oxide in 1 M alkaline solution). Electrochemical impedance spectroscopy (EIS) measurements were performed in a frequency range from 0.1 to 10^4 Hz with AC amplitude of 10 mV under applied bias range from 0.4 V to 0.6 V versus SCE with a scan step of 20 mV.

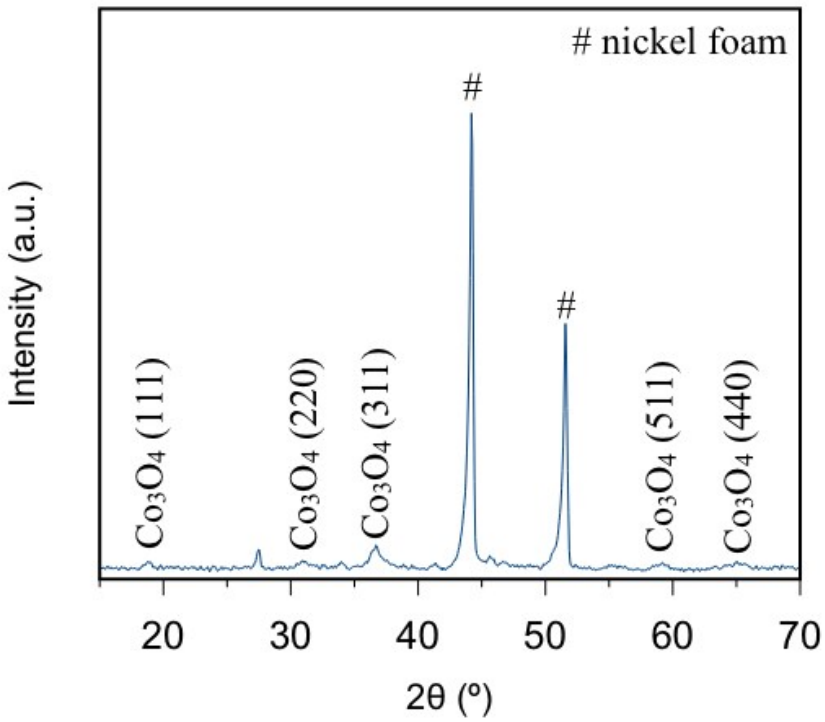

Fig. S1. X-ray diffraction patterns of Co_3O_4 nano-needles on nickel foam.

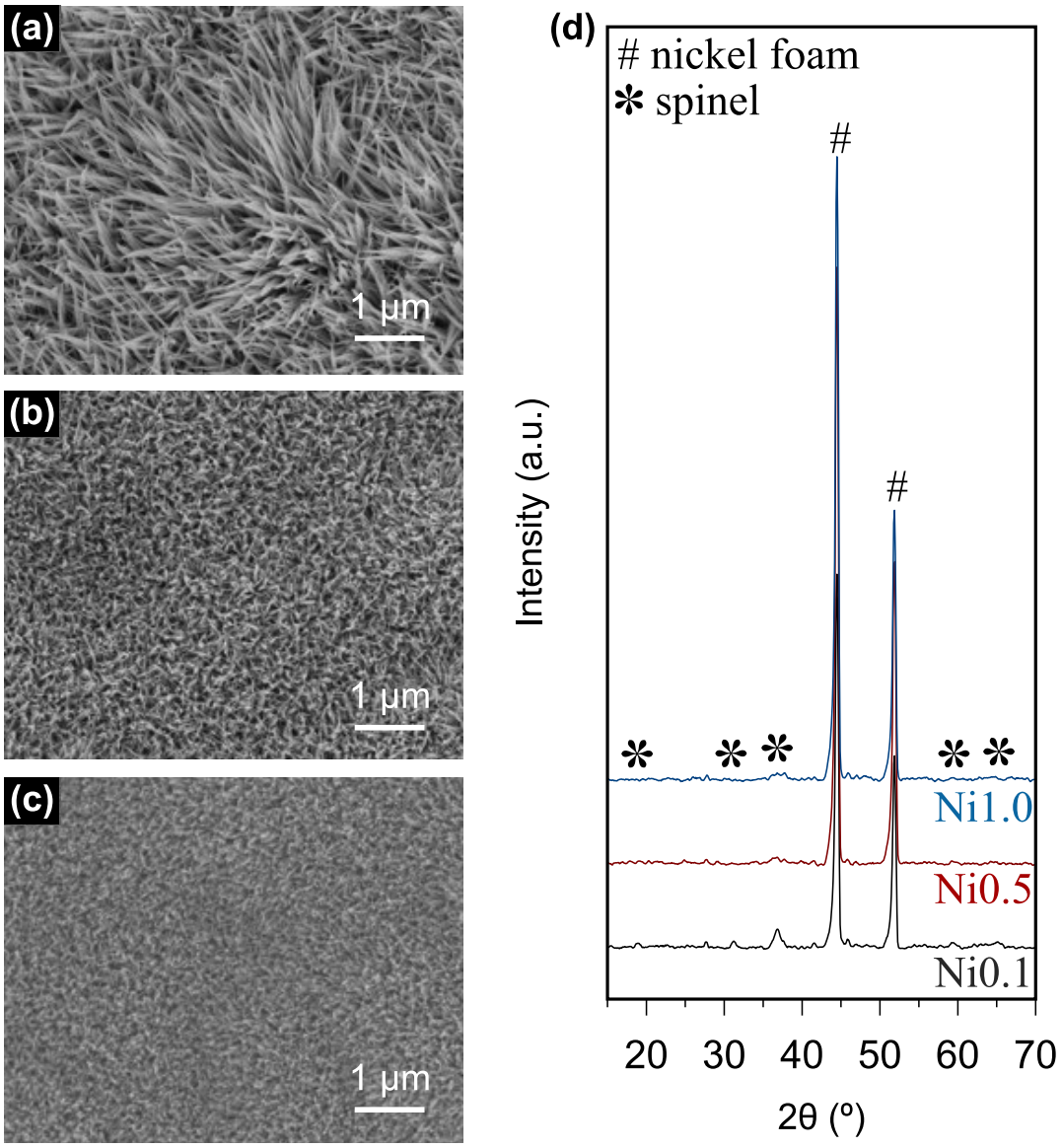

Fig. S2. Microstructure image of Ni-doping Co_3O_4 nano-blanket: The introduction of (a) 0.015 M $Ni(NO_3)_2$ (Ni0.1), (b) 0.075 M $Ni(NO_3)_2$ (Ni0.5), (c) 0.15 M $Ni(NO_3)_2$ (Ni1.0), and the corresponding X-ray diffraction patterns. The lattice constant of cobalt oxide is 8.169 Å (a-axis) (referring to JCPDS #80-1545) while that of nickel oxide is 8.353 Å (a-axis) (referring to JCPDS #89-5881), so that solid solution still existed even when the content of nickel became higher.

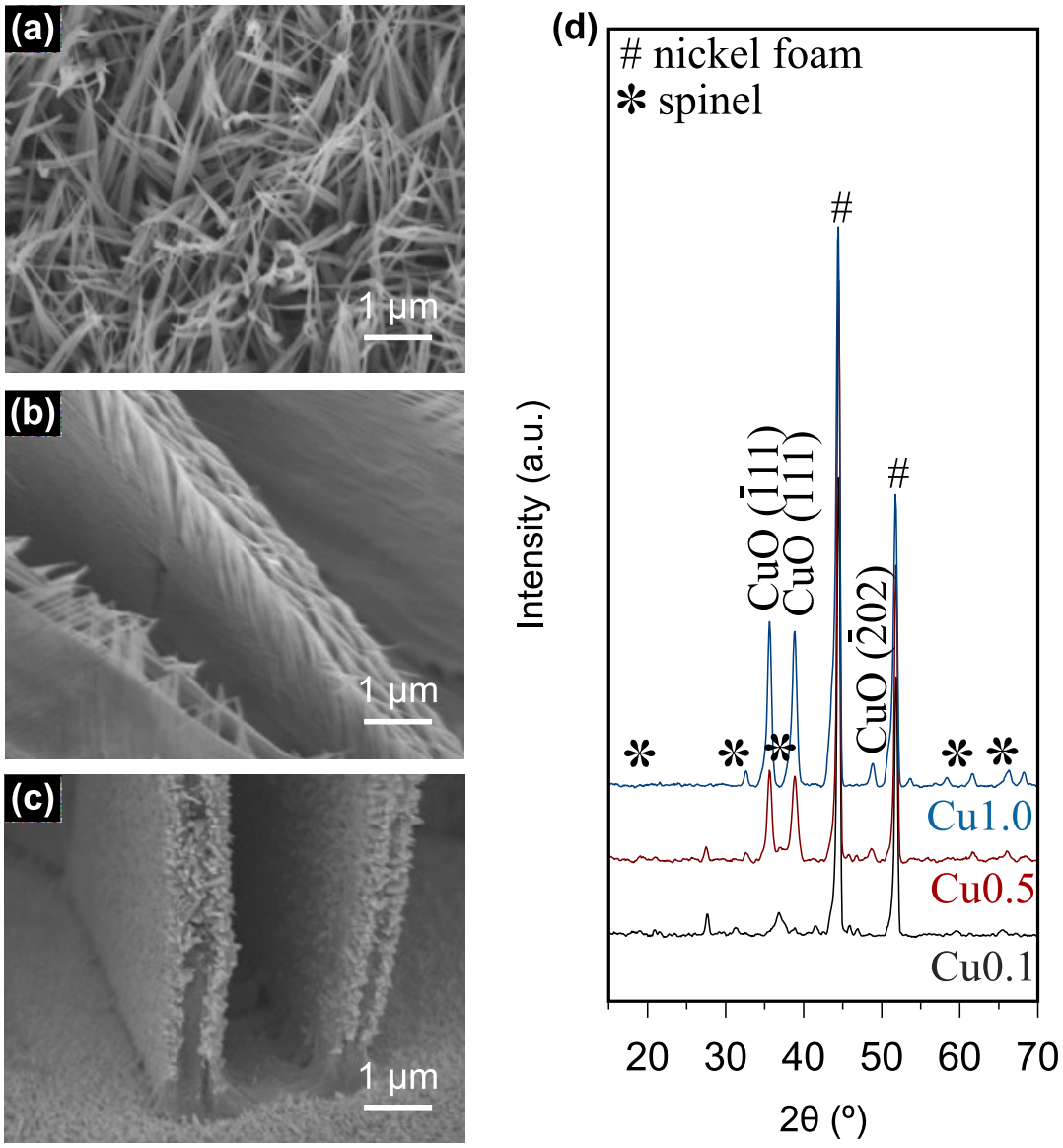

Fig. S3. Microstructure image of Cu-based Co_3O_4 micro-plates: The introduction of (a) 0.015 M $Cu(NO_3)_2$ (Cu0.1), (b) 0.075 M $Cu(NO_3)_2$ (Cu0.5), (c) 0.15 M $Cu(NO_3)_2$ (Cu1.0), and the corresponding X-ray diffraction patterns. The lattice constant of cobalt oxide is 8.169 Å (a-axis) (referring to JCPDS #80-1545) while that of copper oxide is 4.689 Å (a-axis), 3.420 Å (b-axis), and 5.130 Å (c-axis) (referring to JCPDS #89-5899), resulting in the fact that phase separation would be detected when the contents of copper in the nanostructures were higher.

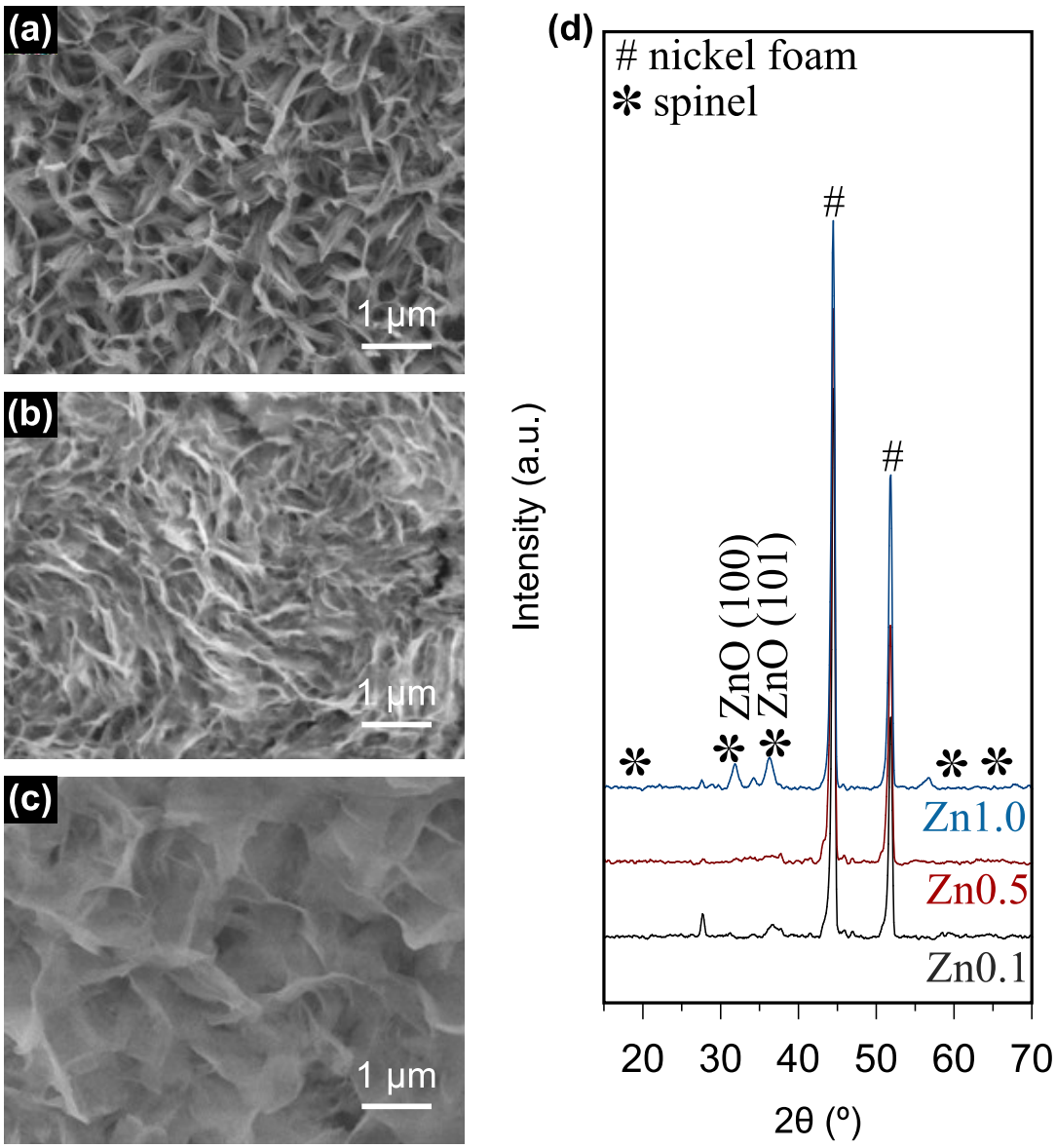

Fig. S4. Microstructure image of Zn-doped Co_3O_4 nano-sheets: The introduction of (a) 0.015 M $Zn(NO_3)_2$ (Zn0.1), (b) 0.075 M $Zn(NO_3)_2$ (Zn0.5), (c) 0.15 M $Zn(NO_3)_2$ (Zn1.0), and the corresponding X-ray diffraction patterns. The lattice constant of cobalt oxide is 8.169 Å (a-axis) (referring to JCPDS #80-1545) while that of zinc oxide is 3.253 Å (a-axis) and 5.213 Å (c-axis) (referring to JCPDS #89-1397), leading to the fact that phase separation would be detected when the contents of zinc in the nanostructures were higher.

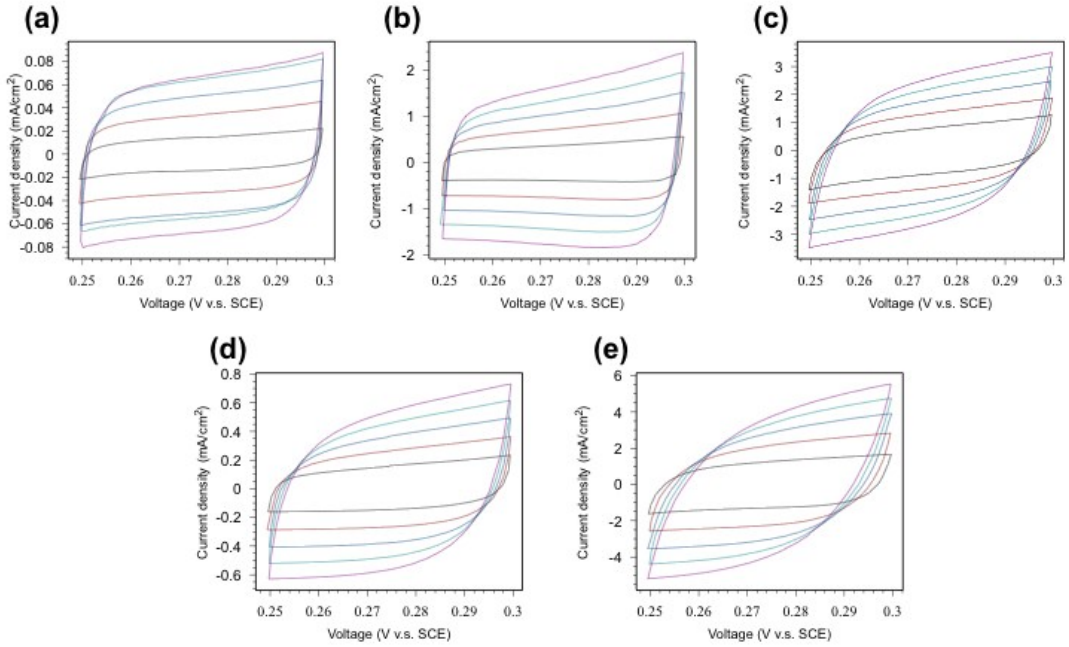

Fig. S5. Cyclic voltammograms in the double layer region at scan rate of 2 mV/s (black line), 4 mV/s (red line), 6 mV/s (blue line), 8 mV/s (green line), and 10 mV/s (purple line) for (a) nickel foam, (b) Co_3O_4 nano-needles, (c) Ni-doped Co_3O_4 nano-blanket, (d) Cu-based Co_3O_4 micro-plates, and (e) Zn-doped Co_3O_4 nano-sheets.

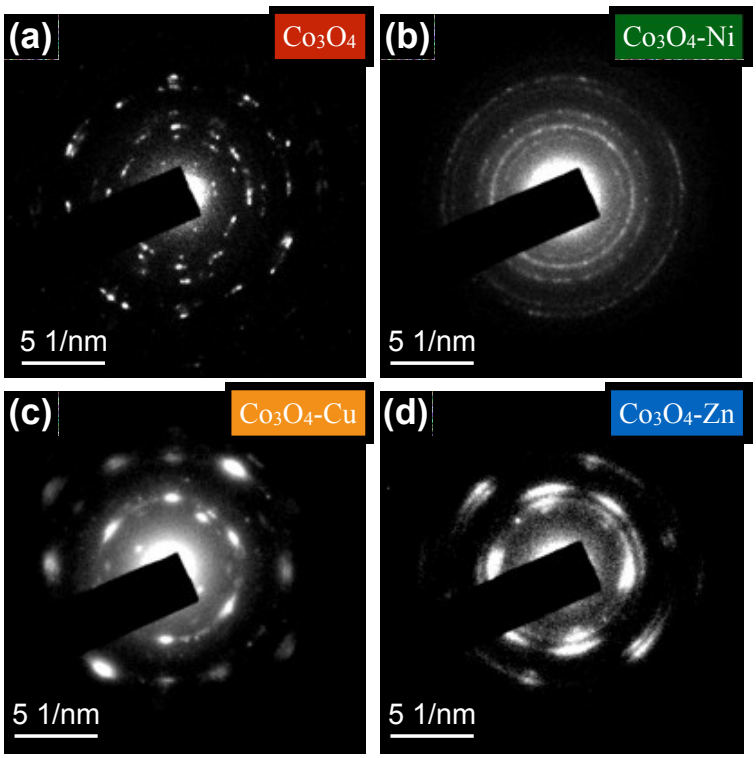

Fig. S6. Selected area electron diffraction for (a) Co_3O_4 nano-needles (b) Ni-doped Co_3O_4 nano-blanket (c) Cu-based Co_3O_4 micro-plates (d) Zn-doped Co_3O_4 nano-sheets. Note that there were the bright spots in the pattern of Cu-based Co_3O_4 micro-plates, which belonged to the pattern of CuO with single crystal and was consistent with the result of XRD.

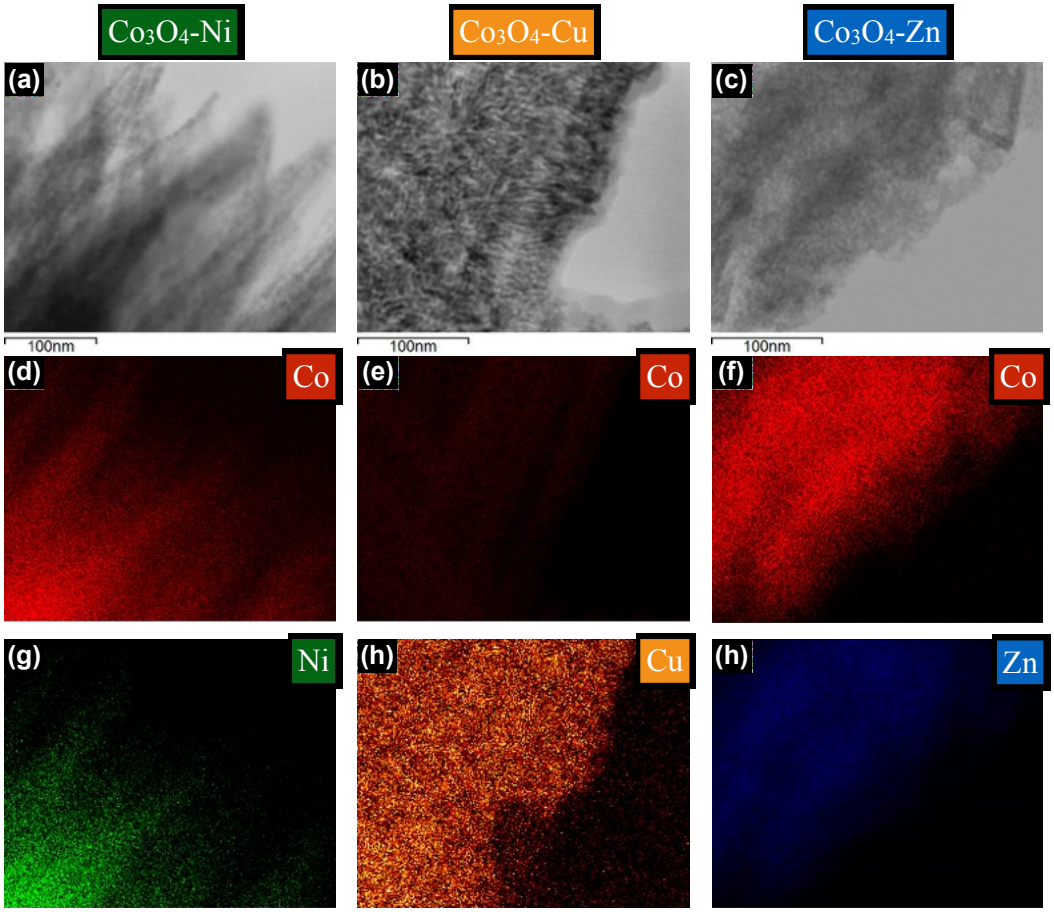

Fig. S7. TEM images of (a) Ni-doped Co_3O_4 nano-blanket (b) Cu-based Co_3O_4 micro-plates (c) Zn-doped Co_3O_4 nano-sheets and the corresponding EDX mapping of each element: (d) Co and (g) Ni for Ni-doped Co_3O_4 nano-blanket; (e) Co and (h) Cu for Cu-based Co_3O_4 micro-plates; (f) Co and (h) Zn for Zn-doped Co_3O_4 nano-sheets.

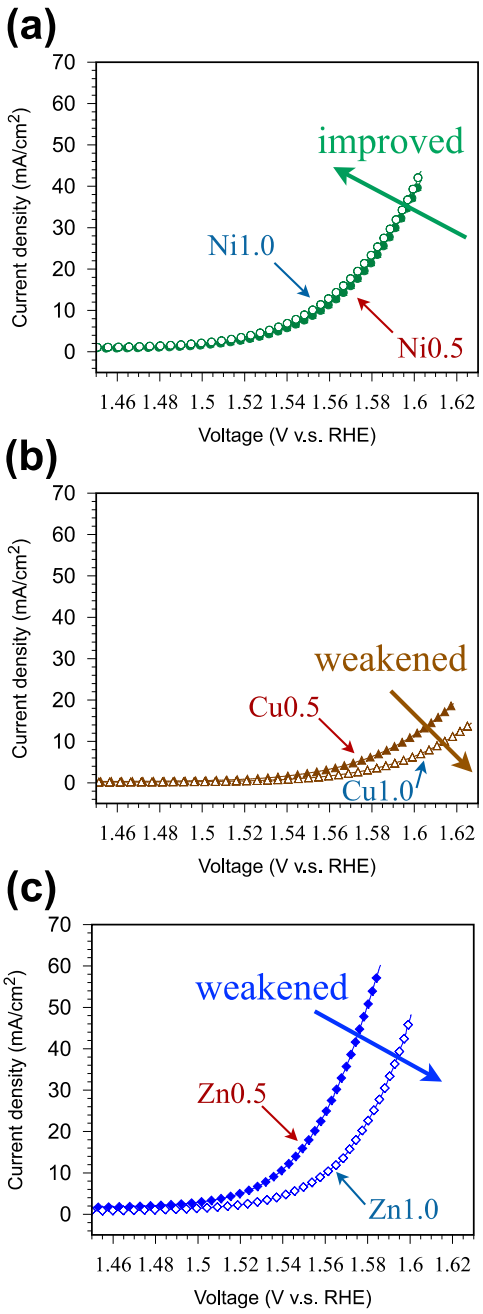

Fig. S8. The comparison of electrochemical activities of cobalt oxide nanostructures with different doping amounts by introducing transition metal nitrates with different concentrationfor oxygen evolution reaction: (a) for nickel, (b) copper, and (c) zinc dopants.

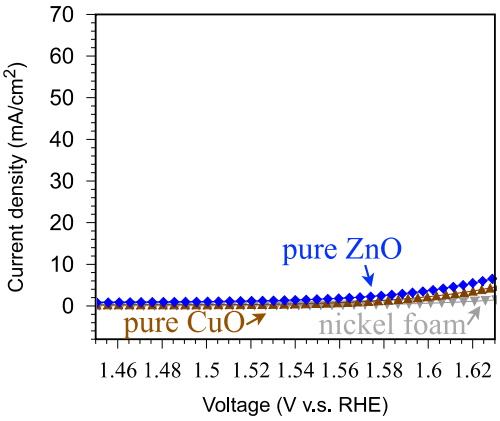

Fig. S9. The electrochemical activities of pure zinc oxide and copper oxide for oxygen evolution reaction, which was conducted by similar chemical bath deposition without introducing cobalt nitrate in the solution.

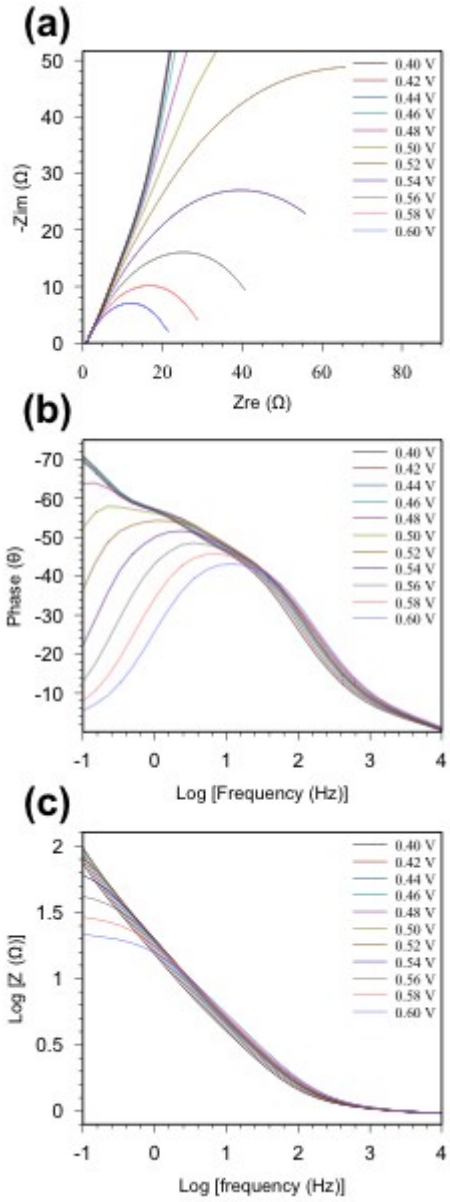

Fig. S10. The electron impedance spectroscopy (EIS) measurement for nickel foam: (a) Nyquist plot, (b) Bode plot, and (c) Bode plot-|*Z*|.

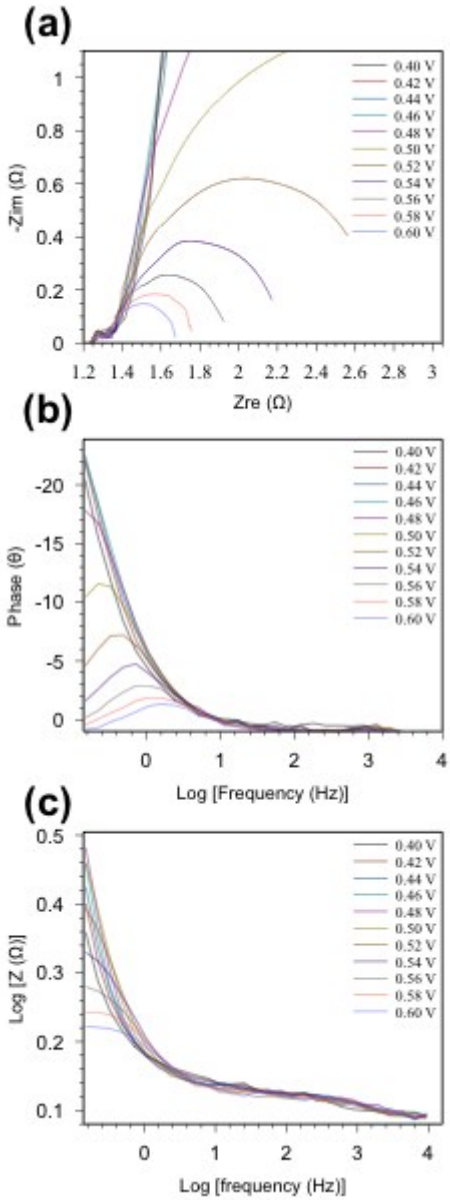

Fig. S11. The electron impedance spectroscopy (EIS) measurement for Co_3O_4 nano-needles: (a) Nyquist plot, (b) Bode plot, and (c) Bode plot-|Z|.

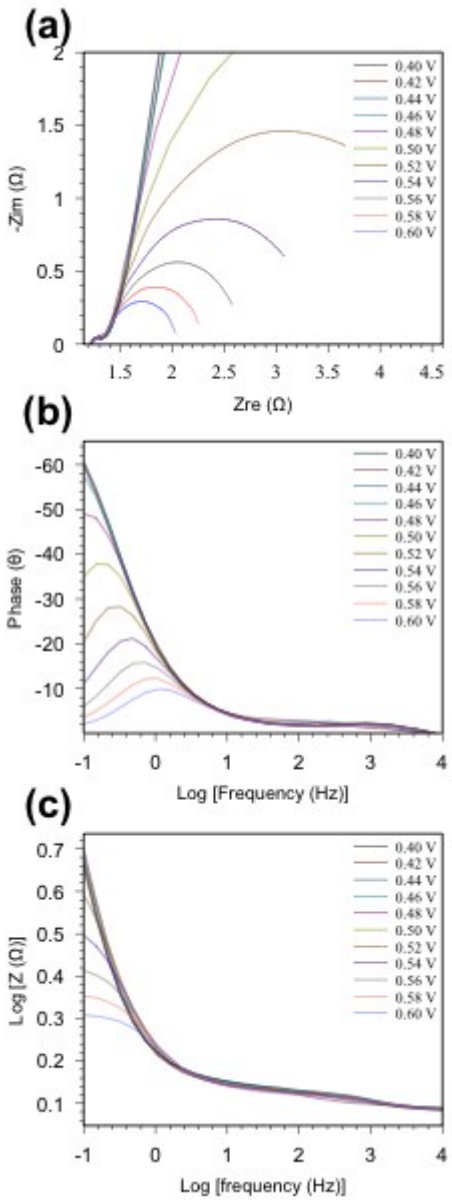

Fig. S12. The electron impedance spectroscopy (EIS) measurement for Ni-doped Co_3O_4 nano-blanket: (a) Nyquist plot, (b) Bode plot, and (c) Bode plot-|Z|.

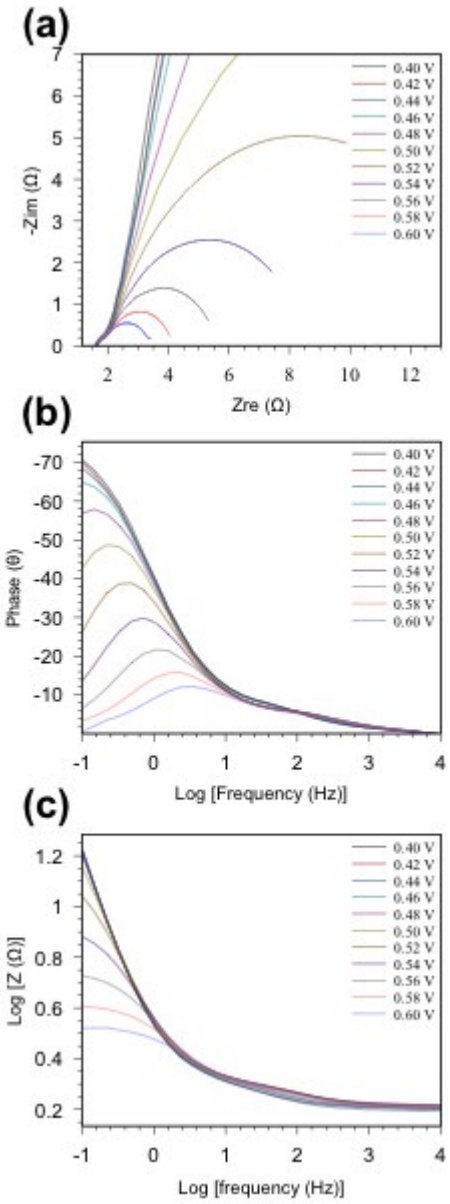

Fig. S13. The electron impedance spectroscopy (EIS) measurement for Cu-based Co_3O_4 micro-plates: (a) Nyquist plot, (b) Bode plot, and (c) Bode plot-|Z|.

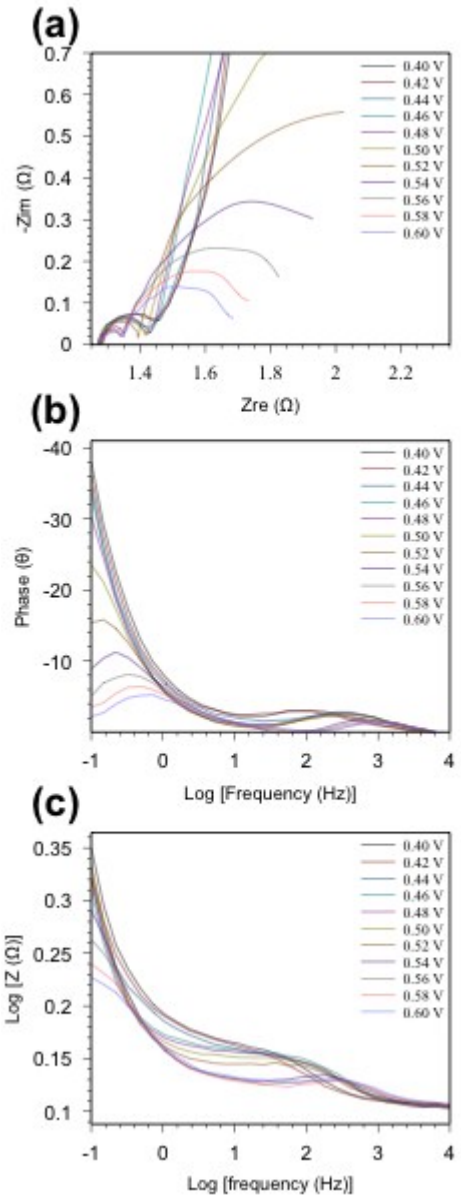

Fig. S14. The electron impedance spectroscopy (EIS) measurement for Zn-doped Co_3O_4 nano-sheets: (a) Nyquist plot, (b) Bode plot, and (c) Bode plot-|Z|.

Table S1. Comparison of over-potential, tafel slope, and roughness factor for various cobalt oxide-based nanostructures.

	Nanostructure	η_{j10} (mV)	tafel slope ($mVdec^{-1}$)	R_f	reference
Co_3O_4	nano-needles	315	58.7	4243	this work
	nano-pillars	440	43	1292	[2]
	nano-rods	450	64	230	[3]
	nano-wires	320	72	7658	[4]
	nano-plates	440	71	n/a	[5]
Co_3O_4-Ni	nano-blackets	322	73.3	5523	this work
	nano-sheets	340	51	680	[3]
	nano-wires	>370	64	3400	[6]
	nano-sponges	362	64.4	n/a	[7]
	nano-cages	340	88	n/a	[8]
	nano-plates	450	n/a	n/a	[9]
Co_3O_4-Cu	micro-plates	365	72.3	1248	this work
	nano-spheres	410	n/a	n/a	[10]
	nanoparticles	400	67	26	[11]
	nanoparticles	>470	63	n/a	[12]
Co_3O_4-Zn	nano-sheets	308	57.2	7915	this work
	nano-pillars	320	51	2512	[2]
	nano-arrays	350	n/a	n/a	[9]
	thin film	390	46	n/a	[13]

References

1 C.-W. Kung, H.-W. Chen, C.-Y. Lin, K.-C. Huang, R. Vittal and K.-C. Ho, *ACS Nano*, 2012, **6**, 7016–7025.

2 X. Liu, Z. Chang, L. Luo, T. Xu, X. Lei, J. Liu and X. Sun, *Chem. Mater.*, 2014, **26**, 1889–1895.

3 H.-Y. Wang, Y.-Y. Hsu, R. Chen, T.-S. Chan, H. M. Chen and B. Liu, *Adv. Energy Mater.*, 2015, **5**, 1500091.

4 P. Chen, K. Xu, Z. Fang, Y. Tong, J. Wu, X. Lu, X. Peng, H. Ding, C. Wu and Y. Xie, *Angew. Chem. Int. Ed.*, 2015, **54**, 14710–14714.

5 X. Zhou, Z. Xia, Z. Tian, Y. Ma and Y. Qu, *J. Mater. Chem. A*, 2015, **3**, 8107–8114.

6 Y. Li, P. Hasin and Y. Wu, *Adv. Mater.*, 2010, **22**, 1926–1929.

7 C. Zhu, D. Wen, S. Leubner, M. Oschatz, W. Liu, M. Holzschuh, F. Simon, S. Kaskel and A. E. X. ller, *Chem.Commun.*, 2015, **51**, 7851–7854.

8 H. Hu, B. Guan, B. Xia and X. W. D. Lou, *J. Am. Chem. Soc.*, 2015, **137**, 5590–5595.

9 X. Zhang, J. Zhang and K. Wang, *ACS Appl. Mater. Interfaces*, 2015, **7**, 21745–21750.

10 A. Serov, N. I. Andersen, A. J. Roy, I. Matanovic, K. Artyushkova and P. Atanassov, *J. Electrochem. Soc.*, 2015, **162**, F449–F454.

11 S. K. Bikkarolla and P. Papakonstantinou, *J. Power Sources*, 2015, **281**, 243–251.

12 X. Wu and K. Scott, *J. Mater. Chem.*, 2011, **21**, 12344.

13 T. W. Kim, M. A. Woo, M. Regis and K.-S. Choi, *J. Phys. Chem. Lett.*, 2014, **5**, 2370–2374.